Oxidative Two-State Photoreactivity of a Manganese(IV) Complex using NIR Light

Nathan R. East[1], Robert Naumann[1], Christoph Förster[1], Charusheela Ramanan[2,3], Gregor Diezemann[1] and Katja Heinze[1]*

[1] Department of Chemistry, Johannes Gutenberg University, Duesbergweg 10-14, 55128 Mainz, Germany. Email: katja.heinze@uni-mainz.de

[2] Department of Physics and Astronomy, Vrije Universiteit Amsterdam, Amsterdam, Netherlands

[3] Max-Planck-Institute for Polymer Research, Mainz, Germany

ORCIDs

Robert Naumann	0000-0002-0912-7644
Christoph Förster	0000-0003-4971-5368
Charusheela Ramanan	0000-0001-8603-6853
Gregor Diezemann	0000-0002-6347-8672
Katja Heinze	0000-0003-1483-4156

Highly reducing or oxidizing photocatalysts are a fundamental challenge in the field of inorganic and organic photochemistry. Only a few transition metal complexes with earth-abundant metal ions have so far advanced to excited state oxidants, including chromium, iron and cobalt. All these photocatalysts require high energy light for excitation and their oxidizing power has not been fully exploited due to significant energy dissipation before reaching the photoactive state. Herein we demonstrate that the complex $[Mn(dgpy)_2]^{4+}$ based on earth-abundant manganese can be excited with low-energy NIR light (850 nm, 1.46 eV) to yield a luminescent mixed ^{2}LMCT/^{2}MC excited state (1435 nm, 0.86 eV) with a lifetime of 1.6 ns. The dissipated energy amounts to 0.60 eV. In spite of this energy loss, $^*[Mn(dgpy)_2]^{4+}$ with its excited state redox potential E_{red}^* of 1.80 V vs SCE outcompetes the strongest reported precious metal photooxidant (iridium(III)). $^*[Mn(dgpy)_2]^{4+}$ oxidizes naphthalene ($E_{ox} \approx 1.31 - 1.54$ V vs. SCE) to its radical cation giving the manganese(III) complex $[Mn(dgpy)_2]^{3+}$ in a clean outer-sphere electron transfer process. Unexpectedly, mesitylene, toluene, benzene and nitriles with even extremely high oxidation potentials up to E_{ox} = 2.4 V provoke the $[Mn(dgpy)_2]^{4+/3+}$ reduction under photolysis. A higher energy short-lived ^{4}LMCT excited state with a lifetime of 0.78 ps is made responsible for these demanding oxidations, which proceed by static rather than dynamic quenching. This dual excited state reactivity from ^{2}LMCT/^{2}MC and ^{4}LMCT states is linked to the ^{4}LMCT → ^{2}LMCT/^{2}MC intersystem crossing process. These unique findings demonstrate how the design of manganese complexes (i) expands the absorption cross section to 400 – 850 nm, (ii) increases the ^{2}LMCT/^{2}MC state lifetime to the nanosecond range allowing luminescence and classical dynamic photoredox processes and (iii) enables non-classical static quenching of an extremely oxidizing ^{4}LMCT excited state by the solvent. This conceptually novel approach of static quenching by the solvent minimizes free energy losses, harnesses the full photooxidizing power and thus allows even oxidation of nitriles and benzene using earth-abundant elements and low-energy light.

The costs of light-harvesting materials represent a bottleneck for widespread implementation, so that the search for novel organic and inorganic materials based on abundant elements is a highly active research field.[1-11] Accepted key requirements for materials in large-scale photochemical applications are a sufficient abundancy on earth, the efficient absorption of visible or even near-IR light, a suitably long excited state lifetime for dynamic quenching, a high photostability and a high stability in different oxidation states both for charge injection at semiconductors or for generating reduced or oxidized substrates in solution reactions.

Complexes of the precious metals fulfil most of these requirements, in particular high excited state lifetimes and reversible redox chemistry. Consequently, photochemical and photovoltaic applications are presently dominated by complexes of ruthenium(II) and iridium(III).[1,11] With respect to photooxidizing properties, many strongly photooxidizing complexes operate as inner-sphere oxidants in hydrogen atom transfer and M–X bond homolysis reactions, such as high valent oxido and halido complexes of manganese(IV), tungsten(VI), cerium(IV), uranium(VI) and copper(II),[12-19] while strong genuine single-electron outer-sphere photooxidants, which fully retain their coordination sphere, are rare. Recent advances in the field of earth-abundant photocatalysts operating as strong single-electron oxidants include zirconium(IV),[20,21] cobalt(III),[22] iron(III)[23-27] and chromium(III) complexes[28-31] in their respective excited states, which are of ligand-to-metal charge transfer character (LMCT)[32] for the former and of spin-flip character for chromium(III) complexes.[10,33]

Photosensitizers possessing excited states with potentials more positive than +0.80 V vs. SCE (+0.42 V vs. ferrocene)[34] are considered as photosensitizers with extreme redox potentials.[35] The strongest iridium(III) containing photooxidant is $[Ir(ppyF_2(CF_3)_2(bpy(CF_3)_2)]^+$ with $E_{red}* = 1.65 – 1.68$ V vs. SCE (1.27 – 1.30 V vs. ferrocene), yet blue LEDs are required for excitation.[35,36] The hexacarbene iron(III) complex $[Fe(phtmeimb)_2]^+$ and various polypyridine chromium(III) complexes realize potentials of $E_{red}* = 1.25 –$ 1.84 V vs. SCE (0.87–1.46 V vs. ferrocene) (phtmeimb = $[phenyl(tris(3\text{-}methylimidazolin\text{-}2\text{-}ylidene))borate]^-$) with blue-green light excitation.[23-31] The formally strongest reported photooxidant based on a first row transition metal is $[Co(dgpz)_2]^{3+}$ with $E_{red}* = 2.75$ V vs. SCE (2.37 V vs. ferrocene), yet its strong oxidizing power towards challenging substrates has not yet been exploited (dgpz = 2,6-diguanidylpyrazine).[22] Strong organic photooxidants encompass substituted acridinium salts,[37] 2,3-dichloro-5,6-dicyano-1,4-benzoquinone[38,39] and the electrochemically generated trisamino-cyclopropenium radical dication with $E_{red}* = 2.06–3.33$ V vs. SCE (1.68–2.95 V vs. ferrocene).[40,41]

To fully harness the photon energy for a redox process, i.e. to reduce the free energy losses after excitation,[42] high energy photoactive states are required for the electron transfer process. Excited states with the same multiplicity as the ground state are typically short-lived, for example organic sensitizers or the iron(III) complex $[Fe(phtmeimb)_2]^+$.[37-41,23,24] Excited states with a multiplicity differing from the ground state multiplicity, for example triplet metal-to-ligand charge transfer states (^{3}MLCT), possess higher excited state lifetimes but are typically at lower energies than the corresponding singlet states (^{1}MLCT) leading to energy dissipation and consequently a loss of oxidizing/reducing power. Furthermore, an intersystem crossing (ISC) process[43] is required to reach the long-lived ^{3}MLCT states, which is often fast and efficient for transition metal complexes, even for first row metals,[44-46] yet in certain cases also slow and inefficient ISC processes have been reported.[47-53]

In the present study we demonstrate that a mixed pyridine/guanidine complex with manganese(IV) as earth-abundant metal ion can be excited with low-energy NIR light to give two photoactive states, namely an unconventional, luminescent and long-lived mixed doublet ligand-to-metal charge transfer/metal-centered (^{2}LMCT/^{2}MC) excited state with some spin-flip admixture at lower energy capable of oxidizing moderately challenging substrates and a short-lived ^{4}LMCT excited state at high energy capable of oxidizing even extremely challenging substrates.

Results and discussion

Ground state properties of $[Mn(dgpy)_2]^{4+}$

The purple-black manganese(IV) complex $[Mn(dgpy)_2][PF_6]_4$ (Fig. 1a) with a d^3 electron configuration yielding a $^4A_2$ ground state (term symbol given for octahedral symmetry) is a strong oxidant in the ground state with $E_{½}(Mn^{IV}/Mn^{III})$ = +0.94 V vs. SCE (0.56 V vs. ferrocene) in acetonitrile (dgpy = 2,6-diguanidylpyridine).[54] One-electron reduction gives the yellow colored high-spin manganese(III) complex $[Mn(dgpy)_2]^{3+}$ (Supplementary Fig. 5).[54] $[Mn(dgpy)_2]^{4+}$ even oxidizes chloride ions in CH_3CN in the dark (Supplementary Fig. 6), similar to the solid state material MnO_2,[55] while light-induced chloride oxidation had been reported using designed ruthenium(II) and organic photooxidants using one- and two-photon excitation mechanisms.[56-58] Clearly, $[Mn(dgpy)_2]^{4+}$ is highly oxidizing already in its ground state and light excitation might even further enhance this oxidizing power.

$[Mn(dgpy)_2][PF_6]_4$ shows panchromatic light absorption throughout the visible spectral region ($\varepsilon_{400–700}$ > 2700 M^{-1} cm^{-1}; Fig. 1a) peaking at 514 nm (6860 M^{-1} cm^{-1}) and 775 nm (sh, 3320 M^{-1} cm^{-1}) and extending into the near-infrared spectral region.[54] On the other hand, the manganese(III) complex $[Mn(dgpy)_2]^{3+}$ absorbs only weakly in the visible spectral region with a weak absorption band at 450 nm (ε = 600 M^{-1} cm^{-1}, Supplementary Fig. 5).[54] According to time-dependent Density Functional Theory (TD-DFT) calculations and charge transfer number analysis, the strong absorption bands of $[Mn(dgpy)_2]^{4+}$ arise from symmetry and spin allowed ^{4}LMCT transitions in particular from the guanidine moieties of the ligands to the high-valent manganese center.[54]

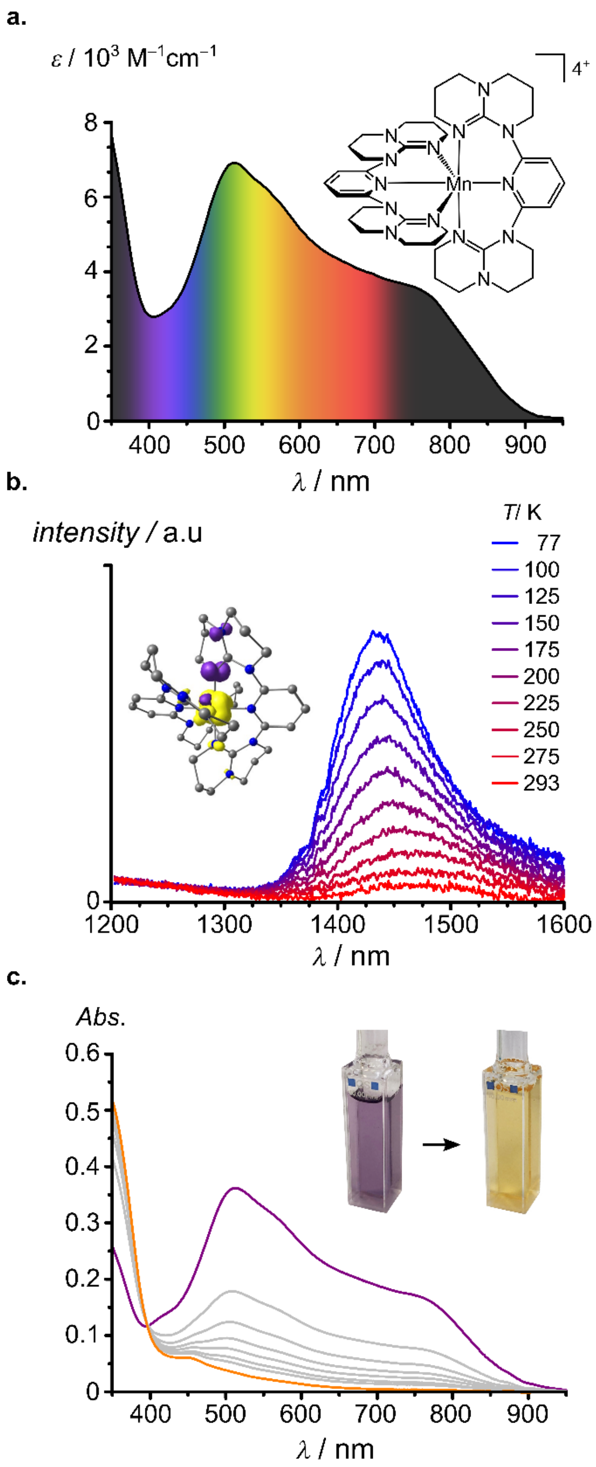

Fig. 1| Steady-state UV/Vis/near-IR and emission spectroscopy of $[Mn(dgpy)_2][PF_6]_4$. a, Absorption spectrum of $[Mn(dgpy)_2][PF_6]_4$ in CH_3CN with the formula of $[Mn(dgpy)_2]^{4+}$ indicated. **b**, Variable temperature luminescence spectra of solid $[Mn(dgpy)_2][PF_6]_4$ after 730 nm excitation and DFT calculated spin density of the lowest ^{2}LMCT/^{2}MC state of $[Mn(dgpy)_2]^{4+}$ at an isosurface value of 0.007 a.u. indicated; α and β spin density in yellow and purple, respectively; hydrogen atoms omitted. **c**, Absorption spectra of $[Mn(dgpy)_2][PF_6]_4$ (50 µM) in CH_3CN in the presence of naphthalene (0.3 M) during 730 nm irradiation over 45 min; the final orange spectrum corresponds to $[Mn(dgpy)_2]^{3+}$ and photographs of the cuvettes before and after irradiation.

Luminescence and excited state reactivity of the doublet state

Laser excitation (635 and 730 nm) of solid [Mn(dgpy)$_2$][PF$_6$]$_4$ resulted in a weak luminescence band around 1470 nm (Fig. 1b, Supplementary Figs. 7,8). Cooling to 77 K lead to a hypsochromic shift of the band of ca. 0.8 cm^{-1} K^{-1} to ca. 1435 nm (0.86 eV) and an approximately tenfold increase in intensity (Fig. 1b). The band is quite sharp with a full width at half maximum (FWHM) of ca. 460 cm^{-1} at 77 K. The only other known luminescent manganese(IV) complex [Mn(phtmeimb)]$^{2+}$ displayed an emission around 828 nm at 85 K with FWHM = 800 cm^{-1} and a hypsochromic of ca. 0.8 cm^{-1} K^{-1} shift from 300 to 85 K.[59] This emission was assigned to the $^2E \rightarrow {}^4A_2$ spin-flip luminescence,[59] although low-energy charge transfer states prevail in the visible spectral region and although the FWHM of the emission band is comparably large.[59] Genuine spin-flip emitters based on chromium(III) exhibit FWHM of the emission bands around 280 and 420 cm^{-1} at room temperature.[60,61]

In contrast to the spin-flip assignment of the [Mn(phtmeimb)]$^{2+}$ luminescence and the similarity of the band characteristics, DFT calculations on the lowest energy doublet state of [Mn(dgpy)$_2$]$^{4+}$ support a strong ^{2}LMCT character with an admixture of metal-centered character (^{2}MC, spin-flip) (Fig. 1b). This mixed ^{2}LMCT/^{2}MC state is calculated at an energy of 0.78 eV above the ground state excellently matching the emission energy of 0.86 eV at 77 K. In the mixed ^{2}LMCT/^{2}MC state, charge has transferred from a coordinated guanidine nitrogen atom to the Mn center (Fig. 1b). Possibly, the admixture of the ^{2}MC state into the ^{2}LMCT state gives rise to a more nested, i.e. less distorted, state and thus a rather sharp emission band. This ^{2}MC admixture giving a weakly distorted excited state might also prolong the doublet state lifetime as has been suggested previously for an oxido manganese(IV) complex.[12]

With the excited doublet state energy of E_{00} = 0.86 eV, the excited state redox potential can be estimated as E^*_{red}(*^{2}Mn^{IV}/Mn^{III}) = 1.80 V vs. SCE (1.42 V vs. ferrocene). This is significantly higher than the excited state redox potential of the strongest reported iridium(III) photooxidant (E^*_{red}(*^{3}Ir^{III}/Ir^{II}) = 1.54 V vs. SCE, 1.16 vs. ferrocene)[35,36] and suffices to oxidize naphthalene with $E_{ox} = \approx 1.31 - 1.54$ V vs. SCE.[12,62] Indeed irradiation of [Mn(dgpy)$_2$][PF$_6$]$_4$ (50 µM) in CH$_3$CN with 730 nm light in the presence of naphthalene (0.3 M) gives the manganese(III) complex according to UV/Vis/NIR spectroscopy (Fig. 1c). The series of spectra during photolysis displays isosbestic points at 334 and 398 nm indicating a clean Mn^{4+} to Mn^{3+} reduction (Fig. 1c). The naphthalene radical cation is too short-lived to be observed under these steady-state conditions. However, the naphthalene radical cation could be trapped by a deactivated pyrazole (1H-pyrazole-4-carboxylic acid ethyl ester) in a Nicewicz-type oxidative coupling.[63,64] The naphthalenyl pyrazole C–H amination product was identified by mass spectrometry (with a signal at m/z = 267 for $C_{16}H_{15}N_2O_2$; Supplementary Fig. 9).

Ultrafast spectroscopy and the excited state reactivity of a quartet excited state

Unexpectedly, irradiation of the complex in the presence of mesitylene, toluene or benzene with much higher oxidation potentials up to E_{ox} = 2.36 V vs. SCE[12,62] and even in pure acetonitrile ($E_{ox} \approx 2.4$ V vs. SCE)[62,65] leads to clean photoreduction, albeit with much slower rates (Supplementary Figs. 10–14). Irradiation of [Mn(dgpy)$_2$][PF$_4$]$_4$ at 730 nm in butyronitrile, nitromethane, 1,2-butylene carbonate or γ-valerolactone with similarly high oxidation potentials[62] as acetonitrile cleanly gives [Mn(dgpy)$_2$]$^{3+}$ as well (Supplementary Figs. 15–18) confirming an extraordinary high oxidation power of *[Mn(dgpy)$_2$]$^{4+}$. The excited state redox potential can be estimated as at least E^*_{red}(*^{4}Mn^{IV}/Mn^{III}) ≈ 2.4 V vs. SCE (≈ 2.0 V vs. ferrocene) based on the CH$_3$CN oxidation potential. With the ground state redox potential given (see above), the excited state energy must be around 1.46 eV. This energy estimation fits to the low-energy tail of the absorption band around 850 nm (1.46 eV, Fig. 1a) and suggests a ^{4}LMCT excited state at E_{00} = 1.46 eV as photoactive state. Indeed, analogous Mn^{4+} to Mn^{3+} photoreductions by CH$_3$CN are observed with 850 nm LED illumination proving that this photoactive excited state of [Mn(dgpy)$_2$]$^{4+}$ is populated even with low energy light (Supplementary Fig. 19).

The proposed initially formed nitrile radical cation $CH_3CN^{\bullet+}$ in acetonitrile can be trapped by an arene, e.g. benzene C_6H_6. Loss of a proton and a further electron yields the corresponding aryl nitrilium ion[66] as shown by ESI mass spectrometry (m/z = 118 for C_8H_8N; Supplementary Fig. 20). Isotopic labeling using C_6D_6 confirms the composition of the generated nitrilium ion (m/z = 123 for $C_8H_3D_5N$; Supplementary Fig. 21). Reaction of activated benzylic C−H bonds with CH_3CN via nitrilium ions had been reported by Lambert to give acetamides after hydrolysis with water using the electrochemically generated photoexcited trisaminocyclopropenium radical dication as oxidant.[67]

To probe the formation of arene radical cations either by direct oxidation with $*[Mn(dgpy)_2]^{4+}$ or by oxidation with the initially formed $CH_3CN^{\bullet+}$ as redox mediator we trapped the arene radical cation by a deactivated electron-poor pyrazole in a Nicewicz-type oxidative coupling.[63,64] Electron-rich arenes have been coupled using 9-mesityl-10-methylacridinium photocatalysts[63,64] and the challenging benzene itself has been coupled using the trisaminocyclopropenium radical dication.[40] Given that transition metal photocatalysts have not been reported to provoke such a transformation, we were pleased to see that mesitylene and even benzene were oxidatively coupled with 1H-pyrazole-4-carboxylic acid ethyl ester using $[Mn(dgpy)_2]^{4+}$ under red-NIR light (730 nm) irradiation to give the respective aminated arenes as shown by ESI mass spectrometry (m/z = 259 for $C_{15}H_{19}N_2O_2$; m/z = 217 for $C_{12}H_{13}N_2O_2$; Supplementary Figs. 22–23). Deuterated benzene gave the isotopologous amination product (m/z = 222 for $C_{12}H_8D_5N_2O_2$, Supplementary Fig. 24). Photolysis (730 nm) of benzene (1.3 M) in CH_3CN with 1H-pyrazole-4-carboxylic acid ethyl ester (30 mM) with $[Mn(dgpy)_2][PF_4]_4$ (2 mM) as the limiting reagent gave 11 % of the coupling product by HPLC analysis (Supplementary Fig. 25).

Cleary, the lowest energy ^{2}LMCT/^{2}MC state at $E_{00}(^2\mathrm{LMCT}/^2\mathrm{MC})$ = 0.86 eV is thermodynamically incompetent to oxidize these arene and nitrile substrates due to its too low excited state redox potential. Consequently, a different excited state must be responsible for this extraordinary photoreactivity, likely a ^{4}LMCT state at an energy $E_{00}(^4\mathrm{LMCT})$ = 1.46 eV, i.e. 0.60 eV higher in energy than the ^{2}LMCT/^{2}MC state. To elucidate the nature of this proposed photoactive ^{4}LMCT state and the excited state dynamics, we performed femtosecond transient absorption (TA) spectroscopy and further mechanistic experiments.

Laser excitation of $[Mn(dgpy)_2][PF_6]_4$ in CH_3CN at 730 nm yields positive excited state absorption (ESA) bands below 420 and above 800 nm and a broad negative band between 430 and 800 nm peaking at 500 nm (Fig. 2a). The spectral evolution of the entire data set was fitted with a global fit comprising of three components with lifetimes of $\tau_{1,2,3}$ = 0.78, 9.7 and 1600 ps (for evolution-associated difference spectra EADS and decay associated difference spectra DADS see Supplementary Fig. 26).

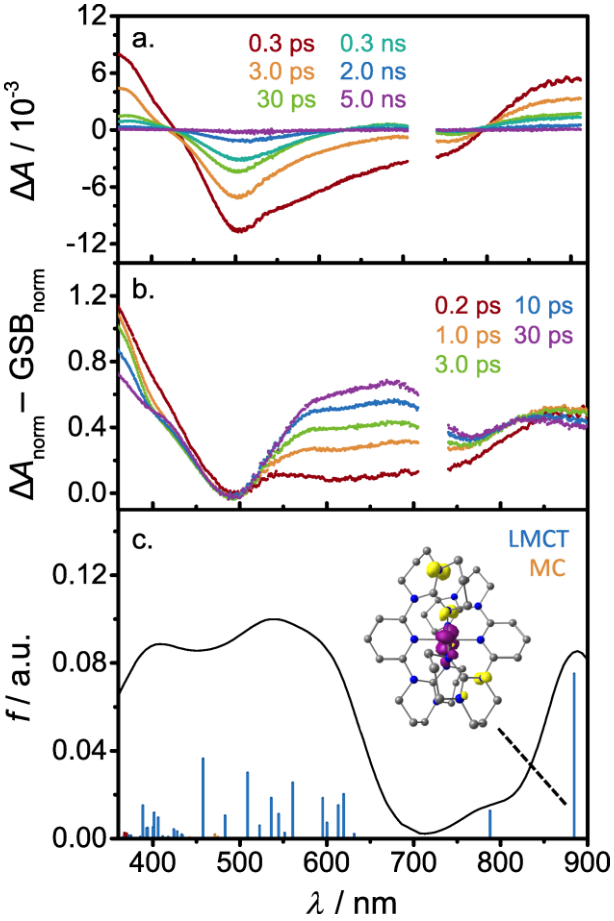

Fig. 2| fs-Transient absorption investigations of [Mn(dgpy)$_2$][PF$_6$]$_4$ in Ar saturated CH$_3$CN revealing the initial formation of the ^{4}LMCT state followed by the slow intersystem crossing to the ^{2}LMCT/^{2}MC state. a, Transient absorption spectra after excitation with 730 nm laser pulses of ca. 200 fs duration (800 nJ / pulse). **b**, Estimated ESA bands and evolution of an additional CT band in the visible range. **c**, Time-dependent DFT calculated low energy spin-allowed transitions of the ^{2}LMCT/^{2}MC state of [Mn(dgpy)$_2$]$^{4+}$ (shifted by 145 cm^{-1} to lower energy) with the color code indicating the character of the transition according to charge transfer number analyses (blue: LMCT, orange: MC; isosurface value of electron difference density at 0.005 a.u., electron gain in purple, electron loss in yellow) and an envelope band shape composed of Gaussians with FWHM of 80 nm.

In general, negative bands can be assigned to the ground state bleach (GSB), although the band shape in most cases strongly deviates from the band shape of the corresponding part of the ground state spectrum due to superimposed ESA bands. For [Mn(dgpy)$_2$][PF$_6$]$_4$, however, the initially observed negative band (t < 300 fs) almost perfectly matches the theoretical GSB spectrum in a large spectral range between 460 and 740 nm (Supplementary Fig. 27). Hence, the ESA of the initially populated ^{4}LMCT state does not contribute significantly to the overall signal in this spectral region. The pure excited state absorption can be estimated by subtracting the normalized theoretical GSB from the normalized difference absorption spectrum. In the spectral region between 460 and 520 nm, the band shape remains even unchanged at all time delays (Supplementary Fig. 27), such that the same method can be employed for all spectra. Fig. 2b displays the resulting ESA spectra revealing the formation of an additional positive band between 500 and 800 nm, which evolves within a few picoseconds and persists, apart from minor band shape changes, until complete relaxation to the ground state. This transition can also be observed in the decay trace at 680 nm, which shows a change of the sign in the original TA data (Supplementary Fig. 28). The formation of this new band indicates a transition from the initially populated ^{4}LMCT state to a new electronically excited state, likely the ^{2}LMCT/^{2}MC state.

Time-dependent DFT calculations of the DFT geometry optimized lowest energy ^{2}LMCT/^{2}MC state (Fig. 1b) find several allowed transitions with predominant LMCT character between 400 and 600 nm as well as between 700 and 900 nm. The overall shape with two discernible absorption bands fits reasonably well to the two ESA bands observed in the TA spectra (Fig. 2c). Thus, we assign this process to the population of the ^{2}LMCT/^{2}MC state via slow ISC with τ_1 = 780 fs. Although ISC is often ultrafast even for 3d transition metal complexes[44-46], it can also be rather slow in the picosecond and even nanosecond range.[47-53] After the population of the ^{2}LMCT/^{2}MC state is completed, the shape of the spectrum remains basically unchanged, besides minor shifts and a small increase of the intensity of the newly formed band (τ_2 = 9.7 ps), which we attribute to thermal relaxation and reorganization of the solvent cage (VR, vibrational relaxation) due to the substantial change of the dipole moment during the LMCT transition. Hence, the slow final decay to the quartet ground state (τ_3 = 1.6 ns) occurs from the thermally relaxed ^{2}LMCT/^{2}MC state. This assignment is also supported by the emission band found at 1435 nm (77 K), which matches the calculated energy of the lowest-energy ^{2}LMCT/^{2}MC state (Fig. 1b, vide supra). Excitation at 350 nm gives the same spectra and lifetime for the long-lived component (τ_1 = 1.6 ns) as obtained with 730 nm excitation (Supplementary Fig. 29). Hence, the ^{2}LMCT/^{2}MC state is populated at both excitation wavelengths showing that no branching occurs at higher energies.

The evolution of the newly formed band could in principle also be rationalized by two other mechanisms, namely formation of low-spin $[Mn(dgpy)_2]^{3+}$ and $CH_3CN^{\bullet+}$ via static hole transfer or by spin crossover (SCO) yielding a ^{6}LMCT state (Supplementary Fig. 30). Hole transfer can be excluded as neither low-spin $[Mn(dgpy)_2]^{3+}$ nor $CH_3CN^{\bullet+}$ show transitions above 450 nm (Supplementary Fig. 31). Furthermore, excitation at 730 nm of $[Mn(dgpy)_2][PF_6]_4$ in CH_3NO_2 gives the same transient absorption spectra (Supplementary Fig. 32) and similar lifetimes ($\tau_{1,2,3}$ = 0.70, 9.1, 1700 ps) illustrating that the spectral evolution is independent of the solvent that is oxidized. SCO to give a ^{6}LMCT state is also unlikely to compete with the ISC as the ^{6}LMCT state is calculated to display merely a single broad absorption band instead of two bands which are experimentally observed. Furthermore, the formation of the ^{6}LMCT state would be accompanied with an elongation of the Mn–N(pyridine) bonds by 0.15–0.26 Å due to the high-spin character of the formal Mn^{3+} center endowing substantial structural reorganization and large barriers.

The suggested sequential relaxation pathway ^{4}LMCT $\rightarrow$ ^{2}LMCT/^{2}MC (hot) $\rightarrow$ ^{2}LMCT/^{2}MC (relaxed) $\rightarrow$ $^4A_2$ nicely fits to the observed reactivity. Challenging substrates like benzene or nitriles must be oxidized before ISC takes place as the ^{2}LMCT/^{2}MC state is not sufficiently oxidizing to enable these reactions (vide supra). Indeed, ISC was found to be comparably slow, such that the static hole transfer to the solvent can compete with the population of the ^{2}LMCT/^{2}MC state. On the other hand, ISC is fast enough to render the hole transfer rather inefficient, which explains the low reaction rate for these substrates. Moreover, the lifetime of the long-lived component remains unaltered when the solvent is changed from CH_3CN to CH_3NO_2 pinpointing the ^{4}LMCT state as the highly reactive excited state. However, the ^{2}LMCT/^{2}MC state combines sufficient oxidative power for less challenging substrates as naphthalene with a nanosecond lifetime that suffices for bimolecular reactivity. The switch from ^{4}LMCT to ^{2}LMCT/^{2}MC reactivity changes the mechanism from a solvent mediated process to direct substrate oxidation.

To confirm that neither dissociated dgpy ligand nor the $[PF_6]^-$ counter ions are potentially reacting with this ^{4}LMCT state we performed several test reactions. Partial ligand dissociation and consequently the presence of traces of dgpy in the solution as potential substrate could be excluded as $[Mn(dgpy)_2]^{4+}$ would oxidize uncoordinated dgpy already in its ground state in the dark (Supplementary Fig. 33). ^{19}F and ^{31}P NMR spectroscopy before and after photolysis confirm that the $[PF_6]^-$ counter ions are not photooxidized as the NMR spectra remain unchanged after photolysis (Supplementary Figs. 34, 35). To further support the redox innocence of the $[PF_6]^-$ counter ions, the perchlorate salt $[Mn(dgpy)_2][ClO_4]_4$ has been prepared and investigated additionally (Supplementary Information). Irradiation of $[Mn(dgpy)_2][ClO_4]_4$ at 730 nm in CH_3CN leads to photoreduction of $[Mn(dgpy)_2]^{4+}$ as well, even slightly faster than with $[PF_6]^-$ counter ions (Supplementary Figs. 36, 37). The molar conductivity of $[Mn(dgpy)_2][PF_6]_4$ in CH_3CN is with 640 S cm^{-1} M^{-1} comparably high (Supplementary Fig. 38), although not many 1:4 electrolytes have been investigated so far hampering comparisons.[68,69] A molecular dynamics simulation of $[Mn(dgpy)_2][PF_6]_4$ in CH_3CN over 1 µs resulted in shells of counterions with $Mn\cdots[PF_6]$ (center-of-mass) distances peaking at 4.1, 6.1, 7.3 and 8.5 Å suggesting ion-pairing with $[PF_6]^-$ ions (Supplementary Fig. 39). Similarly, the molar conductivity of $[Mn(dgpy)_2][PF_6]_3$ in CH_3CN (560 S cm^{-1} M^{-1}) is high for a 1:3 electrolyte (Supplementary Fig. 38).[68,69] To probe the effect of ion paring on the photoreduction and cage escape,[70] $[Mn(dgpy)_2][PF_6]_4$ was photolyzed in CH_3CN in the presence of increasing amounts of $[n\text{-}Bu_4N][PF_6]$ (0, 50, 100 and 200 mM; Supplementary Figs. 40–42). The reaction is significantly slowed down with increasing $[PF_6]^-$ concentration suggesting a slower photooxidation of CH_3CN or a slower cage escape at high ionic strength (Supplementary Fig. 43). As the ultrafast dynamics observed by TA spectroscopy are unaffected by the presence of 100 mM $[n\text{-}Bu_4N][PF_6]$ (Supplementary Fig. 44), we suggest that the initial static quenching is not hampered but rather the cage escape reaction at high ionic strength. A similar retarding effect on the photoreduction, likely also affecting the cage escape rate, occurs when diluting the acetonitrile solution with redox-inert ortho-dichlorobenzene in 1:1 and 1:2 v/v ratios (Supplementary Figs. 45–47).

These combined experiments support the conclusion that the redox partner of the ^{4}LMCT excited Mn^{4+} complex is the solvent itself. Solvent molecules are already present in the vicinity of the Mn^{4+} complex. Two short $Mn\cdots N(CH_3CN)$ distances of 4.91 and 5.73 Å are present in the solid state structure (CCDC-2171816).[54] The molecular dynamics simulation of $[Mn(dgpy)_2][PF_6]_4$ in CH_3CN over 1 µs resulted in shells of CH_3CN molecules around the tetracation with $Mn\cdots[CH_3CN]$ (center-of-mass) distances peaking at ca. 3.9, 6.0, 8.5, 12.3 and 16.8 Å (Supplementary Fig. 48). The first peak up to 4.25 Å corresponds to 0.9 CH_3CN molecules, i.e. approximately one CH_3CN molecule is present close to the Mn center. This allows for static quenching of the short-lived ^{4}LMCT state competitive with ISC, while a purely dynamic quenching on the short time scale of the ^{4}LMCT lifetime would be highly unlikely. Consequently, the reactivity of $[Mn(dgpy)_2]^{4+}$ in its excited ^{4}LMCT state relies on the extremely high excited state potential sufficient for solvent oxidation by a static quenching mechanism.

Quantum chemical calculations and mechanistic picture

Optical excitation of $[Mn(dgpy)_2]^{4+}$ from its $^4A_2$ ground state yields ^{4}LMCT excited Franck-Condon states at energies from to 1.4 to 3.0 eV (Fig. 1a). The lowest-energy absorptions are assigned to the ^{4}LMCT transitions calculated at 656 and 637 nm shown in Fig. 3a with their electron difference densities. In these ^{4}LMCT states, electron density has been transferred from the guanidine ligands to a d_π orbital (t_{2g} in O_h notation) of the manganese center, i.e. forming a guanidine radical cation and a manganese(III) ion in its low-spin electron configuration.

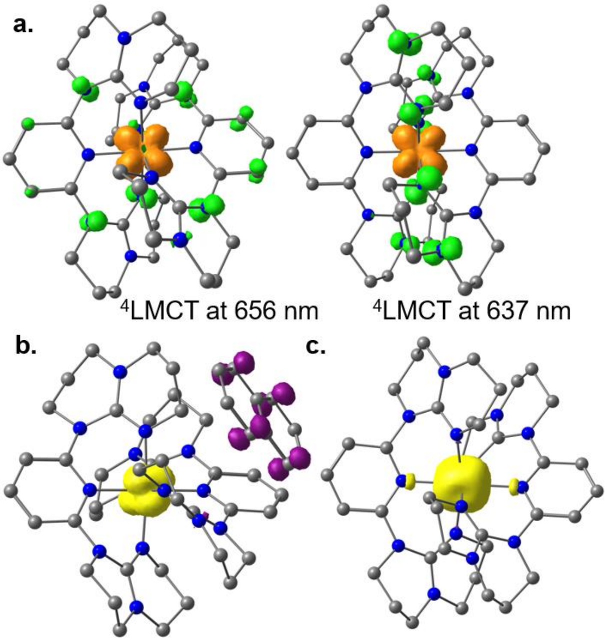

Fig. 3 | Quantum chemical calculations of excited states of $[Mn(dgpy)_2]^{4+}$ and the products of the photoinduced electron transfer reaction. a, Difference electron density of the two lowest spin-allowed ^{4}LMCT transitions at 656 and 637 nm (green = electron density loss; orange = electron density gain) displayed at an isosurface value of 0.006 a.u.. **b**, DFT optimized geometry of the $^2\{[Mn(dgpy)_2]^{3+}/\text{naphthalene}^{\bullet+}\}^{4+}$ pair with spin densities after the electron transfer showing the low-spin $[Mn(dgpy)_2]^{3+}$ complex and the naphthalene radical cation. **c**, DFT optimized geometry and spin density of the high-spin $[Mn(dgpy)_2]^{3+}$ complex. Spin densities at an isosurface value of 0.012 a. u.; α and β spin density in yellow and purple, respectively. Hydrogen atoms omitted.

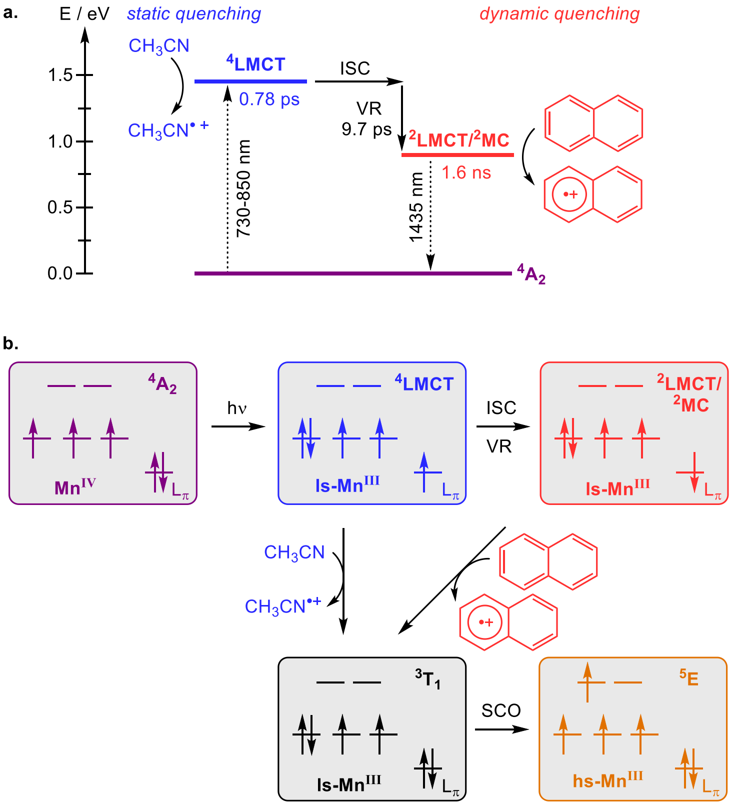

Fig. 4 | Jablonski diagram and electron configurations of the involved excited states and redox states. **a**, Jablonski diagram including photoinduced redox processes from the ^{4}LMCT and ^{2}LMCT/^{2}MC excited states with acetonitrile and naphthalene, respectively, including data from luminescence and TA spectroscopy; ISC = intersystem crossing, VR = vibrational relaxation. **b**, Electron configurations of the $^4A_2$ ground state (purple), ^{4}LMCT (blue) and ^{2}LMCT/^{2}MC (red) excited states and the low-spin (black, $^3T_1$) and high-spin (orange, ^{5}E) manganese(III) complexes illustrated by the occupation of metal 3d orbitals and a ligand π orbital (L_π) (SCO = spin crossover).

The lifetime of the populated ^{4}LMCT state depends on the rates of the static quenching by a CH_3CN solvent molecule and of the ISC to the doublet manifold (Fig. 4a). With the above interpretations resulting from the TA spectra, the ISC process is rather slow in this Mn^{4+} complex. Still, only static quenching by the solvent accounts for the excited state reactivity of the ^{4}LMCT state. Hole transfer gives the acetonitrile radical cation and the low-spin manganese(III) complex ($^3T_1$, Fig. 4b). The latter is only weakly distorted compared to the manganese(IV) complex suggesting only a small kinetic barrier to hole transfer. The low-spin complex can then undergo spin-crossover (SCO) to the thermodynamically favored high-spin complex (^{5}E, Fig. 4b).[54] The here suggested oxidation of the solvent as initial photoredox step likely also occurs with other extremely strong photooxidants (which short excited state lifetimes) such as the electrochemically generated trisaminocyclopropenium radical dication in CH_3CN.[40,41] Yet, this static quenching scenario of short-lived strongly oxidizing excited states by the solvent had not been considered so far.

The ^{2}LMCT/^{2}MC excited state resulting from ISC and vibrational relaxation is at lower energy by 0.60 V (Fig. 4a). Hypothetically pure ^{2}MC excited doublet states ($^2E/^2T_1$ spin-flip states) neglecting charge-transfer admixtures as assigned in the reported carbene manganese(IV) complex $[Mn(phtmeimb)_2]^{2+}$ [59] are expected around 572 and 540 nm for $[Mn(dgpy)_2]^{4+}$ according to CASSCF/NEVPT2 calculations comprising only the d orbitals.[54] Clearly, these putative pure spin-flip states are too high in energy to be the lowest energy doublet states in $[Mn(dgpy)_2]^{4+}$ but these spin-flip states can obviously mix with the ^{2}LMCT state. Hole transfer from the mixed ^{2}LMCT/^{2}MC state to a naphthalene substrate was modelled by DFT calculations generating the manganese(III) complex and the substrate radical cation (Figs. 3b, 4a). Spin conservation requests that the d^4 Mn^{III} complex forms in its low-spin state ($S_{Mn} = 1$, $^3T_1$) with the radical cation spin ($S_{radical} = {}^1/_2$) antiferromagnetically coupled to give a spin-correlated pair with $S_{total} = {}^1/_2$ (Fig. 3b). The Mn–N bond lengths increase only slightly from 1.95 – 1.98 Å in the ^{2}LMCT/^{2}MC state to 2.00 Å in the highly symmetric low-spin $[Mn(dgpy)_2]^{3+}$ complex. This small elongation suggests only a minor reorganization energy stemming from the photooxidant for the hole transfer reaction. The initially formed low-spin manganese(III) complex finally undergoes SCO to yield the high-spin complex with $S_{Mn} = 2$ (^{5}E, Fig. 3c, 4b). The Mn–N(pyridine) bonds are significantly elongated to 2.20 Å in the high-spin configuration, and hence a larger structural reorganization likely occurs in the SCO step only after the actual hole transfer.

Conclusions

The high-valent manganese(IV) complex $[Mn(dgpy)_2]^{4+}$ constitutes the prototype of a new class of extremely potent outer-sphere photooxidants. The panchromatic absorption, the high ground state redox potential, the small reorganization energy of the $[Mn(dgpy)_2]^{4+}$/low-spin $[Mn(dgpy)_2]^{3+}$ couple and the unique dual excited state reactivity of a 3d transition metal complex resulting from static quenching of a short-lived highly oxidizing ^{4}LMCT state and from dynamic quenching of a long-lived luminescent strongly oxidizing ^{2}LMCT/^{2}MC state allow for oxidations including challenging substrates such as nitriles and benzene, using low-energy red to near-infrared light (730 nm, 850 nm). The novel key aspects of this unique system are the exploitation of the earth-abundant, non-noble metal manganese instead of precious metals such as iridium, the usage of red to near-infrared light instead of the typically used UV to green light for oxidative transformations, the minimal dissipative energy loss and the resulting extremely high excited state redox potential sufficient for solvent oxidation as the primary hole transfer step. Future studies will explore adapted and tuned $^*Mn^{4+}/Mn^{3+}$ couples as photo(electro)catalysts in challenging transformations e.g. via ion pairing and as sensitizers for suitable p-type semiconductors close to the thermodynamic and kinetic limits.

Online content

Any methods, additional references, Nature Research reporting summaries, source data, extended data, supplementary information, acknowledgements, peer review information; and competing interests; and statements of data and code availability are available at xx.

Author contributions

N.R.E. performed the syntheses, the reactivity studies, the photolysis experiments and the computational studies. R.N. performed and analyzed the luminescence and ultrafast time-resolved experiments and provided data interpretation. C.F. performed and assisted with the computational studies. C.R. assisted with the time-resolved experiments. G.D. performed and analyzed the molecular dynamics simulations. K.H. conceptualized the research, conceived the experiments and performed data analyses and interpretation. All authors co-wrote the manuscript.

Conflict of interest

The authors declare no conflict of interest.

Methods

See the Supplementary Information for full details of the methods employed.

Data Availability

All data generated or analyzed during this study are included in this published article or its Supplementary Information files, which include Cartesian coordinates of DFT optimized geometries, photolyses under various conditions (light sources, substrates), luminescence and transient absorption spectroscopic data, conductivity data.

Acknowledgements

This work was supported by the Max Planck Graduate Center with the Johannes Gutenberg University Mainz (MPGC). N.R.E. is a recipient of a position through the DFG Excellence Initiative by the Graduate School Materials Science in Mainz (GSC 266). This work was further supported by the Deutsche Forschungsgemeinschaft through grant INST 247/1018-1 FUGG to KH. Parts of this research were conducted using the supercomputer Mogon and advisory services offered by Johannes Gutenberg University Mainz (http://www.hpc.uni-mainz.de) and the supercomputer Elwetritsch and advisory services offered by the Rheinland-Pfälzische Technische Universität Kaiserslautern-Landau (https://hpc.rz.rptu.de), which are members of the AHRP and the Gauss Alliance e.V.. We thank Dimitri Zorn for performing the HPLC analyses.

References

1. Prier, C. K., Rankic, D. A. & MacMillan, D. W. C. Visible light photoredox catalysis with transition metal complexes: applications in organic synthesis. *Chem. Rev.* **113**, 5322–5363 (2013).
2. Romero, N. A. & Nicewicz, D. A. Organic Photoredox Catalysis. *Chem. Rev.* 116, 10075−10166 (2016).

3. Liu, Y. Z., Persson, P., Sundström, V. & Wärnmark, K. Fe N-heterocyclic carbene complexes as promising photosensitizers. *Acc. Chem. Res.* **49**, 1477−1485 (2016).
4. Larsen, C. B. & Wenger, O. S. Photoredox catalysis with metal complexes made from earth-abundant elements. *Chem. Eur. J.* **24**, 2039–2058 (2018).
5. Wenger, O. S. Photoactive complexes with earth-abundant metals. *J. Am. Chem. Soc.* **140**, 13522–13533 (2018).
6. Otto, S., Dorn, M., Förster, C., Bauer, M., Seitz, M. & Heinze, K. Understanding and Exploiting Long-lived Near-infrared Emission of a Molecular Ruby. *Coord. Chem. Rev.* **359**, 102–111 (2018).
7. Förster, C. & Heinze, K. Photophysics and photochemistry with Earth-abundant metals – fundamentals and concepts. *Chem. Soc. Rev.* **49**, 1057–1070 (2020).
8. Dierks, P., Vukadinovic, Y. & Bauer, M. Photoactive iron complexes: more sustainable, but still a challenge. *Inorg. Chem. Front.* **9**, 206−220 (2022).
9. Kitzmann, W. R., Ramanan, C., Naumann, R. & Heinze, K. Molecular Ruby: Exploring the Excited State Landscape. *Dalton Trans.* **51**, 6519–6525 (2022).
10. Kitzmann, W. R., Moll, J. & Heinze, K. Spin-Flip Luminescence. *Photochem. Photobiol. Sci.* **21**, 1309–1331 (2022).
11. Sinha, N. & Wenger, O. S. Photoactive Metal-to-Ligand Charge Transfer Excited States in 3d^6 Complexes with Cr^0, Mn^I, Fe^{II}, and Co^{III}. *J. Am. Chem. Soc.* **45**, in press (2023). DOI: 10.1021/jacs.2c13432.
12. Sharma, N., Jung, J., Ohkubo, K., Lee, Y.-M., El-Khouly, M. E., Nam, W . & Fukuzumi, S. Long-Lived Photoexcited State of a Mn(IV)-Oxo Complex Binding Scandium Ions That is Capable of Hydroxylating Benzene. *J. Am. Chem. Soc.* **140**, 8405−8409 (2018).
13. Tzirakis, M. D., Lykakis, I. N. & Orfanopoulos, Decatungstate as an efficient photocatalyst in organic chemistry. *Chem. Soc. Rev.* **38**, 2609–2621 (2009).
14. Yu, D., To, W.-P., Tong, G. S. M., Wu, L.-L., Chan,K.-T., Du, L., Phillips, D. L., Liu, Y. & Che, C.-M. Luminescent tungsten(VI) complexes as photocatalysts for light-driven C–C and C–B bond formation reactions. *Chem. Sci.* **11**, 6370–6382 (2020).
15. Zhang, K., Chang, L., An, Q., Wang, X. & Zuo, Z. Dehydroxymethylation of Alcohols Enabled by Cerium Photocatalysis. *J. Am. Chem. Soc.* **141**, 26, 10556–10564 (2019).
16. Yang, Q., Wang, Y.-H., Qiao, Y., Gau, M., Carroll, P. J., Walsh, P. J. & Schelter, E. J. Photocatalytic C–H activation and the subtle role of chlorine radical complexation in reactivity. *Science* **372**, 847–852 (2021).
17. Yatham, V. R., Bellotti,P. & König, B. Decarboxylative hydrazination of unactivated carboxylic acids by cerium photocatalysis. *Chem. Commun.* **55**, 3489–3492 (2019).
18. West, J. G., Bedell, T. A. & Sorensen, E. J. The Uranyl Cation as a Visible-Light Photocatalyst for C(sp^3)–H Fluorination. *Angew. Chem. Int. Ed.* **55**, 8923–8927 (2016).
19. Abderrazak, Y., Bhattacharyya, A. & Reiser, O. Visible-Light-Induced Homolysis of Earth-Abundant Metal-Substrate Complexes: A Complementary Activation Strategy in Photoredox Catalysis. *Angew. Chem. Int. Ed.* **60**, 21100–21115 (2021).
20. Zhang, Y., Petersen, J. L. & Milsmann, C. A Luminescent Zirconium(IV) Complex as a Molecular Photosensitizer for Visible Light Photoredox Catalysis. *J. Am. Chem. Soc.* **138**, 13115−13118 (2016).
21. Zhang, Y., Lee, T. S., Petersen, J. L. & Milsmann, C. A zirconium photosensitizer with a long-lived excited state: mechanistic insight into photoinduced single-electron transfer. *J. Am. Chem. Soc.* **140**, 5934–5947 (2018).
22. Pal, A.K., Li, C., Hanan, G.S. & Zysman-Colman, E. Blue-Emissive Cobalt(III) Complexes and Their Use in the Photocatalytic Trifluoromethylation of Polycyclic Aromatic Hydrocarbons. *Angew. Chem. Int. Ed.* **57**, 8027–8031 (2018).

23. Chábera, P. et al. A low-spin Fe(III) complex with 100-ps ligand-to-metal charge transfer photoluminescence. *Nature* **543**, 695–699 (2017).
24. Kjær, K. S. et al. Luminescence and reactivity of a charge-transfer excited iron complex with nanosecond lifetime. *Science* **363**, 249–253 (2019).
25. Rosemann, N. W., Chábera, P., Prakash, O., Kaufhold, S., Wärnmark, K., Yartsev, A. & Persson, P. Tracing the Full Bimolecular Photocycle of Iron(III)−Carbene Light Harvesters in Electron-Donating Solvents. *J. Am. Chem. Soc.* **142**, 8565−8569 (2020).
26. Aydogan, A., Bangle, R. E., Cadranel, A., Turlington, M. D., Conroy, D. T., Cauët, E., Singleton, M. L., Meyer, G. J., Sampaio, R. N., Elias, B. & Troian-Gautier, L. Accessing Photoredox Transformations with an Iron(III) Photosensitizer and Green Light. *J. Am. Chem. Soc.* **143**, 15661−15673 (2021).
27. Steube, J., Kruse, A., Bokareva, O. S., Reuter, T., Demeshko, S., Schoch, R., Cordereo, M. A. A., Krishna, A., Hohloch, S., Meyer, F., Heinze, K., Kühn, O., Lochbrunner, S. & Bauer, M. Janus-type emission of a Cyclometalated Iron(III) complex. Nat. Chem. (2023). DOI: 10.1038/s41557-023-01137-w.
28. Stevenson, S. M., Shores, M. P. & Ferreira, E. M. Photooxidizing Chromium Catalysts for Promoting Radical Cation Cycloadditions. *Angew. Chem. Int. Ed.* **54**, 6506 –6510 (2015).
29. Sittel, S., Naumann, R. & Heinze, K. Molecular Rubies in Photoredox Catalysis. *Front. Chem.* **10**, 887439 (2022).
30. Bürgin, T. H., Glaser, F. & Wenger, O. S. Shedding Light on the Oxidizing Properties of Spin-Flip Excited States in a Cr^{III} Polypyridine Complex and Their Use in Photoredox Catalysis. *J. Am. Chem. Soc.* **144**, 14181–14194 (2022).
31. Sittel, S., Sell, A. C. Hofman, K., Wiedemann, C., Nau, J. P., Kerzig, C., Manolikakes, G. & Heinze, K. Visible-Light Induced Fixation of SO_2 into Organic Molecules with Polypyridine Chromium(III) Complexes. *Chem. Cat. Chem.* in press (2023). DOI: 10.1002/cctc.202201562.
32. Li, C., Kong, X. Y., Tan, Z. H. Yang, C. T. & Soo, H. S. Emergence of ligand-to-metal charge transfer in homogeneous photocatalysis and photosensitization. *Chem. Phys. Rev.* **3**, 021303 (2022).
33. Förster, C. & Heinze, K. Bimolecular Reactivity of 3d Metal-Centered Excited States (Cr, Mn, Fe, Co). *Chem. Phys. Rev.* **3**, 041302 (2022).
34. Connelly, N. G. & Geiger, W. E. Chemical Redox Agents for Organometallic Chemistry. *Chem. Rev.* **96**, 877–910 (1996).
35. Kim, D. & Teets, T. S. Strategies for accessing photosensitizers with extreme redox potentials. *Chem. Phys. Rev.* **3**, 021302 (2022).
36. Choi, G. J., Zhu, Q., Miller, D. C., Gu, C. J. & Knowles, R. R. *Nature* **539**, 268 (2016).
37. Tlili, A. & Lakhdar, S. Acridinium Salts and Cyanoarenes as Powerful Photocatalysts: Opportunities in Organic Synthesis. *Angew. Chem. Int. Ed.* **60**, 19526–19549 (2021).
38. Natarajan, P. & König, B. Excited-State 2,3-Dichloro-5,6-dicyano-1,4-benzoquinone (DDQ*) Initiated Organic Synthetic Transformations under Visible-Light Irradiation. *Eur. J. Org. Chem.* 2145–2161 (2021).
39. Huang, H. & Lambert, T. H. Electrophotocatalytic SNAr Reactions of Unactivated Aryl Fluorides at Ambient Temperature and Without Base. *Angew. Chem. Int. Ed.* **59**, 658–662 (2020).
40. Huang, H., Strater, Z. M., Rauch, M., Shee, J., Sisto, T. J., Nuckolls, C. & Lambert, T. H. Electrophotocatalysis with a Trisaminocyclopropenium Radical Dication. *Angew. Chem. Int. Ed.* **58**, 13318–13322 (2019).
41. Huang, H. & Lambert, T. H. Electrophotocatalytic Acetoxyhydroxylation of Aryl Olefins. *J. Am. Chem. Soc.* **143**, 7247–7252 (2021).

42. Cotic, A., Cerfontaine, S., Slep, L. D., Elias, B., Troian-Gautier, L. & Cadranel, A. Anti-Dissipative Strategies toward More Efficient Solar Energy Conversion. *J. Am. Chem. Soc.* (2023). DOI: 10.1021/jacs.2c11593.
43. Penfold, T. J., Gindensperger, E., Daniel, C. & Marian, C. M. Spin-Vibronic Mechanism for Intersystem Crossing. *Chem. Rev.* **118**, 6975–7025 (2018).
44. Auböck, G. & Chergui, M. Sub-50-fs photoinduced spin crossover in $Fe(bpy_3)^{2+}$. *Nat. Chem.* **7**, 629−633 (2015).
45. Juban, E. A. & McCusker, J. K. Ultrafast Dynamics of ^2E State Formation in $Cr(acac)_3$. *J. Am. Chem. Soc.* **127**, 6857-6865 (2005).
46. Wang, C., Reichenauer, F., Kitzmann, W. R., Kerzig, C., Heinze, K., Resch-Genger, U. Efficient Triplet-Triplet Annihilation Upconversion Sensitized by a Chromium(III) Complex via an Underexplored Energy Transfer Mechanism. *Angew. Chem. Int. Ed.* **61**, e202202238 (2022).
47. Dose, E.V., Hoselton, M. A., Sutin, N., Tweedle, M. F. & Wilson, L. J. Dynamics of Intersystem Crossing Processes in Solution for Six-Coordinate d^5, d^6, and d^7 Spin-Equilibrium Metal Complexes of Iron(III), Iron(II), and Cobalt(II). *J. Am. Chem. Soc.* **100**, 1141–1147 (1978).
48. Siddique, Z. A., Yamamoto, Y., Ohno, T. & Nozaki, K. Structure-Dependent Photophysical Properties of Singlet and Triplet Metal-to-Ligand Charge Transfer States in Copper(I) Bis(diimine) Compounds. *Inorg. Chem.* **42**, 6366–6378 (2003).
49. Iwamura, M., Takeuchi, S. & Tahara, T. Real-Time Observation of the Photoinduced Structural Change of Bis(2,9-dimethyl-1,10-phenanthroline)copper(I) by Femtosecond Fluorescence Spectroscopy: A Realistic Potential Curve of the Jahn-Teller Distortion. *J. Am. Chem. Soc.* **129**, 5248–5256 (2007).
50. Shaw, G. B., Grant, C. D., Shirota, H., Castner Jr., E. W., Meyer, G. J. & Chen, L. X. Ultrafast Structural Rearrangements in the MLCT Excited State for Copper(I) bis-Phenanthrolines in Solution. *J. Am. Chem. Soc.* **129**, 2147–2160 (2007).
51. Gonçalves, P.J. De Boni, L., Borissevitch, I. E. & Zílio, S. C. Excited State Dynamics of meso-Tetra(sulphonatophenyl) Metalloporphyrins. *J. Phys. Chem. A* **112**, 6522–6526 (2008).
52. Dorn, M., Kalmbach, J., Boden, P., Päpcke, A., Gómez, S., Förster, C., Kuczelinis, F., Carrella, L. M., Büldt, L., Bings, N., Rentschler, E., Lochbrunner, S., González, L., Gerhards, M., Seitz, M., & Heinze, K. A vanadium(III) complex with blue and NIR-II spin-flip luminescence in solution. *J. Am. Chem. Soc.* **142**, 7947–7955 (2020).
53. Antolini, C., Spellman, Jr., C. D., Otolski, C. J., Doumy, G., March, A. M., Walko, D. A., Liu, C., Zhang, X., Young, B. T., Goodwill, J. E. & Hayes, D. Photochemical and Photophysical Dynamics of the Aqueous Ferrate(VI) Ion. *J. Am. Chem. Soc.* **144**, 22514−22527 (2022).
54. East, N. R., Förster, C., Carrella, L. M., Rentschler, E. & Heinze, K. The full d^3–d^5 Redox Series of Mononuclear Manganese Complexes: Geometries and Electronic Structures of $[Mn(dgpy)_2]^{n+}$. *Inorg. Chem.* **61**, 14616–14625 (2022).
55. A. F. Holleman, F. Wiberg, Lehrbuch der anorganischen Chemie, 101. Ed., Walter de Gruyter Verlag, Berlin, New York, 1995
56. Troian-Gautier, L., Turlington, M. D., Wehlin, S. A. M., Maurer, A. B., Brady, M. D., Swords, W. D. & Meyer, G. J. Halide Photoredox Chemistry. *Chem. Rev.* **119**, 4628−4683 (2019).
57. Ward, W. M., Farnum, B. H., Siegler, M. & Meyer, G. J. Chloride Ion-Pairing with Ru(II) Polypyridyl Compounds in Dichloromethane. *J. Phys. Chem. A* **117**, 8883−8894 (2013).
58. Li, P., Deetz, A. M., Hu, J., Meyer, G. J. & Hu, K. Chloride Oxidation by One- or Two-Photon Excitation of N-Phenylphenothiazine. *J. Am. Chem. Soc.* **144**, 17604−17610 (2022).
59. Harris, J. P.; Reber, C.; Colmer, H. E.; Jackson, T. A.; Forshaw, A. P.; Smith, J. M.; Kinney, R. A. & Telser, J. Near-infrared ^2E_g - $^4A_{2g}$ and visible LMCT luminescence from a molecular bis-(tris(carbene)borate) manganese(IV) complex. *Can. J. Chem.* **95**, 547−552 (2017).

60. Reichenauer, F., Wang, C., Förster, C., Boden, P., Ugur, N., Báez-Cruz, R., Kalmbach, J., Carrella, L. M., Rentschler, E., Ramanan, C., Niedner-Schatteburg, G., Gerhards, M., Seitz, M., Resch-Genger, U. & Heinze, K. Strongly Red-Emissive Molecular Ruby $[Cr(bpmp)_2]^{3+}$ surpasses $[Ru(bpy)_3]^{2+}$. *J. Am. Chem. Soc.* **143**, 11843–11855 (2021).
61. Otto, S., Grabolle, M., Förster, C., Kreitner, C., Resch-Genger, U. & Heinze, K. $[Cr(ddpd)_2]^{3+}$: a molecular, water-soluble, highly NIR-emissive ruby analogue. *Angew. Chem. Int. Ed.* **54**, 11572–11576 (2015).
62. Fundamentals and Applications of Organic Electrochemistry (Eds. Fuchigami, T., Inagi, S., Atobe, M.), John Wiley & Sons, Ltd, 2015, Appendix B.
63. Romero, N. A., Margrey, K. A., Tay, N. E. & Nicewicz, D. A. Site-selective arene C-H amination via photoredox catalysis. *Science* 2015, **349**, 1326–1330.
64. Pistritto, V. A., Liu, S. & Nicewicz, D. A. Mechanistic Investigations into Amination of Unactivated Arenes via Cation Radical Accelerated Nucleophilic Aromatic Substitution. *J. Am. Chem. Soc.* **144**, 15118–15131 (2022).
65. Foley, J. K., Korzeniewski, C. & Pons, S. Anodic and cathodic reactions in acetonitrile/tetra-n-butylammonium tetrafluoroborate: an electrochemical and infrared spectroelectrochemical study. *Can. J. Chem.* **66**, 201–206 (1988).
66. Hammerich, O. & Parker, V. D. Reaction of the Anthracene Cation Radical with Acetonitrile. A Novel Anodic Acetamidation. *J. Chem. Soc., Chem. Commun.* 245–246, (1974).
67. Shen, T. & Lambert, T. H. C−H Amination via Electrophotocatalytic Ritter-type Reaction. *J. Am. Chem. Soc.* **143**, 8597–8602 (2021).
68. Geary, W. J. The use of conductivity measurements in organic solvents for the characterisation of coordination compounds. *Coord. Chem. Rev.* **7**, 81–122 (1971).
69. Basu, U., Otto, S., Heinze, K. & Gasser, G. Biological Evaluation of the NIR-Emissive Ruby Analogue $[Cr(ddpd)_2][BF_4]_3$ as a Photodynamic Therapy Photosensitizer. *Eur. J. Inorg. Chem.* 37–41 (2019).
70. Kavarnos, G. J. & Turro, N. Photosensitization by Reversible Electron Transfer: Theories, Experimental Evidence, and Examples. *Chem. Rev.* **86**, 401–449 (1986).